15th IFK
Proc. of the 15th International Fluid Power Conference <Symposium/Conference>
<DOI>

Development and Experimental Validation of a Novel Origami-Inspired Pneumatic Actuator Concept with Progressive Force-Stroke Characteristics

Philipp Hüpper, Olivier Reinertz, Katharina Schmitz

RWTH Aachen University, Institute for Fluid Power Drives and Systems, Aachen, Germany, philipp.huepper@ifas.rwth-aachen.de

Abstract.

Pneumatic actuators currently face limitations in achieving a progressive correlation between force and stroke under isobaric conditions. This characteristic bears the potential to significantly improve applications such as vibration isolation, which benefits from minimal stiffness and low eigenfrequency, and automation, where reduced air consumption can be achieved, e.g., in clamping devices. Conventional actuator designs struggle to provide these features because they require the active area to increase with the stroke.

This paper deals with a novel origami-inspired actuator concept, which offers a promising solution by increasing the active area progressively over its stroke. The primary challenge lies in the structure's design. From a mathematical point of view, origami actuators with rigid facets represent shape-variable polyhedrons, which are isochoric despite a possible form change, making them unsuitable as pneumatic actuators. However, engineering approaches demonstrate that slight elongations of selected edges during form change can enable significant volume changes. The goal is to overcome technical challenges by developing an airtight origami structure that transmits force along its facets and edges while permitting minor facet deviations.

A working prototype is designed, manufactured and experimentally investigated on a force-stroke test rig. Measurement results validate the feasibility of the concept and the achievement of the targeted properties.

Keywords. origami, pneumatic, actuators, design, progressive force actuators

1. INTRODUCTION

Origami is the art of paper folding. Although origami was traditionally used for artistic purposes, it found technical applications in the 20th century [1]. Examples include space-efficient, folded structures for rocket transportation [2]; medical products, such as stents [3]; and foldable concrete structures designed to achieve high local stiffness [4]. Complex patterns are created by introducing mountain and valley folds into a sheet of paper [5]. This results in rigid facets connected by movable creases. Points where these creases meet are referred to as vertices [5].

In a new approach, Reinertz demonstrated that origami can be used for designing a pneumatic actuator chamber with a progressive force-stroke characteristic. By inverting the principle of a bellow actuator, this approach utilizes rigid facets to transmit force while allowing deformation along the creases. Currently, no commercially available pneumatic actuators offer a progressive stroke characteristic, though such actuators would be highly beneficial for suspension systems due to their low eigenfrequency and could contribute to energy savings in automation. [6]

This paper will turn this new approach, as shown in Figure 1.1.a), into a working prototype. Manufacturing difficulties will be solved by tailoring the mechanical properties of Reinertz's proposed geometry. An experimental investigation will demonstrate the desired progressive force-stroke characteristic of the actuator, which could result in a low eigenfrequency.

Sadeghi et al. already employed origami techniques to develop a quasi-zero stiffness pneumatic actuator [7]. The proof-of-concept prototype revealed both the desired progressive force-stroke characteristic and low eigenfrequency [8]. However, this design lacks practicality because the end facets of the used Miura-Ori origami change significantly in size during actuation, as shown in Figure 1.1.b). This is not beneficial for a pneumatic actuator because the required sliding seals between the facets and adjacent end faces induce significant amounts of leakage and friction. Additionally, the point of force application moves relative to the end faces.

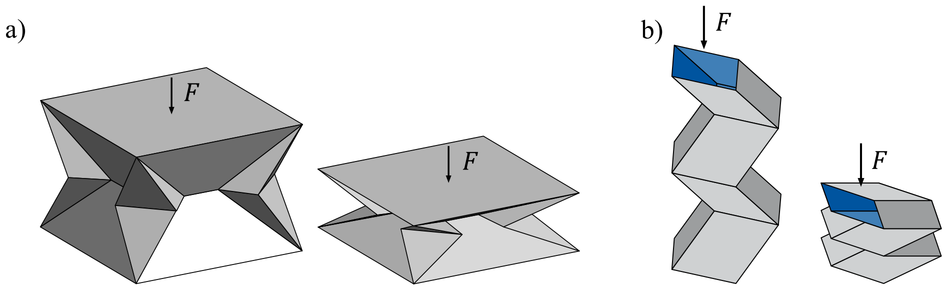

Figure 1.1. a) Reinertz's proposed geometry [6]; b) origami structure of Sadeghi et al. [7]

Building upon Reinertz's approach, the goal is to create a polyhedron whose facets do not change during deformation [6]. From a mathematical perspective, however, it is impossible to alter the volume of a deformable closed polyhedron without changing its facet shapes [9], making such structures infeasible as pneumatic actuators. Nevertheless, Reinertz's design creates a change in volume through slight deviations from a mathematically exact polyhedron, achieved by the elasticity of a few creases [6].

The scope of this paper is to first optimize the proposed geometry for manufacturing a working prototype. After analyzing critical points, the origami pattern will be optimized numerically to minimize facet deformation. The manufactured prototype will finally be tested on a testbed to characterize the pneumatic properties of the actuator, focusing on the force stroke correlation under isobaric conditions.

2. ANALYSIS OF CRITICAL POINTS

To further improve feasibility, the proposed geometry, shown in Figure 2.1.a), is slightly modified. For the realization of technical origami structures, vertices are critical points since multiple creases converge there. The complexity of sealing and force transmission increases as the number of meeting creases increases. As shown in Figure 2.1.b), one way to reduce this complexity is by lowering the maximum number of creases that meet at each vertex. The size of these new facets can be tailored so that the pneumatic properties of the actuators remain comparable.

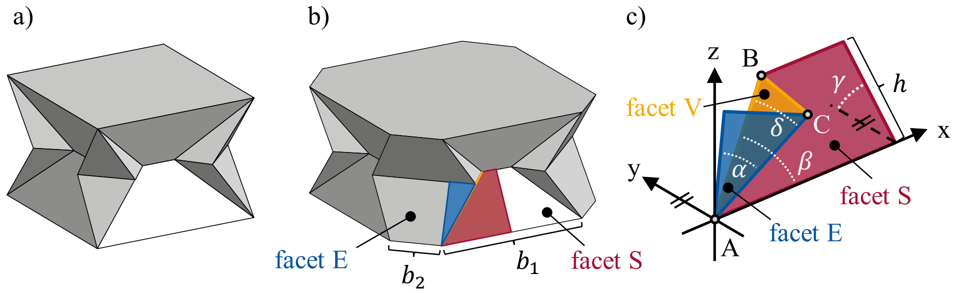

Figure 2.1. a) Reinertz's proposed geometry [6]; b) modified geometry; c) one vertex of the origami-pattern

For analytical purposes, the structure can be simplified to a single vertex, as illustrated in Figure 2.1.c). This reduction is possible because the entire actuator structure can be formed by reflecting this vertex multiple times. In this configuration, the facets are labeled E, S, and V with corresponding angles α, β, and δ. The actuator stroke is defined by angle γ. For clarity in further discussions, key points A, B, and C are also marked.

In a classic origami pattern, angles α, β, and δ are related by Equation 2.1 and do not change. This relation is not effective for a functional actuator. As Reinertz demonstrated, an actuator can be created by allowing a small elongation of the crease $\overline{BC}$ [6]. Therefore, the angle δ must change during actuation.

$$\alpha + \beta + \delta = 90° \tag{2.1}$$

The goal is to minimize stress on facet V and its connecting creases, as well as to simplify manufacturing, by keeping changes in δ as small as possible. The alteration in δ over a full actuator stroke is defined as $\Delta\delta$ by Equation 2.2:

$$\Delta\delta = \delta_{\max} - \delta_{\min} \tag{2.2}$$

Here, δ_{max} is the maximum value of δ during the actuator stroke, and δ_{min} is the corresponding minimum value. Minimizing $\Delta\delta$ requires numerical optimization of the angles α, β, and δ. This optimization process will be discussed in detail in the following section.

3. Numerical Optimization of the Origami Pattern

To minimize $\Delta\delta$, a geometric analysis is required to describe the angle δ as a function of the other geometric parameters and the actuator stroke. The distances between points A, B, and C ($\overline{AB}$, $\overline{AC}$ and $\overline{BC}$) are defined as shown in Equations 3.1 to 3.3:

$$\overline{AB} = h \cdot \sqrt{\left(\frac{1}{\tan\beta}\right)^2 + \cos^2\gamma + \sin^2\gamma} \tag{3.1}$$

$$\overline{AC} = h \cdot \sqrt{\frac{1}{2}(\cos\gamma + \tan\alpha)^2 + \frac{1}{2}(\cos\gamma - \tan\alpha)^2 + \sin^2\gamma} \tag{3.2}$$

$$\overline{BC} = h \cdot \sqrt{\left(\frac{1}{\tan\beta} - \frac{\sqrt{2}}{2}(\cos\gamma + \tan\alpha)\right)^2 + \left(\cos\gamma - \frac{\sqrt{2}}{2}(\cos\gamma - \tan\alpha)\right)^2} \tag{3.3}$$

Using the law of cosines, the angle δ can be calculated by Equation 3.4:

$$\delta(\alpha, \beta, \gamma) = \arccos\left(\frac{\overline{AB}^2 + \overline{AC}^2 - \overline{BC}^2}{2 \cdot \overline{AB} \cdot \overline{AC}}\right) \tag{3.4}$$

$\delta(\alpha, \beta, \gamma)$ is independent of the height h, as it is eliminated. By choosing values for α and β, δ can be determined depending on γ. It can be shown that δ follows a trajectory similar to Figure 3.1.c). As γ approaches zero, $\frac{\partial\delta}{\partial\gamma}$ also approaches zero. Depending on the values of α and β, δ reaches a minimum before always increasing as γ approaches 90°, which represents the maximal possible stroke.

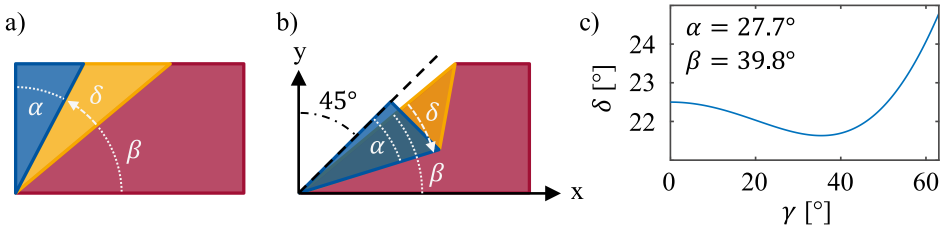

Figure 3.1. Exemplary course of $\boldsymbol{\delta}$ over the stroke $\boldsymbol{\gamma}$

To maximize the stroke while minimizing changes in δ, γ could theoretically be set near zero or around the minimum point of δ. However, setting γ close to zero is not technically feasible because it would cause actuator components to intersect. Therefore, γ is defined as $\gamma = [21°, 45.8°]$. This range includes the minimum point of δ and allows for a maximal stroke that is twice as large as the minimal stroke.

To ensure that the structure closely resembles origami, the relationship given by Equation 2.1 is taken into consideration. This relationship guarantees that the origami pattern can be folded from a flat sheet of paper, as illustrated in Figure 3.1.a). The pattern can be folded according to Figure 2.1.c). When the pattern is folded flat ($\gamma = 0°$), Figure 2.1.c) becomes Figure 3.1.b) when viewed from above. Then, α, β, and δ have the relationship given by Equation 3.5:

$$\alpha + \beta - 45° = \delta \tag{3.5}$$

Equating Equation 2.1 and Equation 3.5 yields $\delta = 22.5°$. Inserting this into Equation 2.1 yields the condition between α and β given by Equation 3.6:

$$\alpha + \beta = 67.5° \tag{3.6}$$

The maximum and minimum values of δ during the stroke $\gamma = [21°, 45.8°]$ are determined using Equation 3.4 with values of α and β that satisfy the condition in Equation 3.6. Then, the change in δ, $\Delta\delta$, is calculated using Equation 2.2.

With $\alpha = 27.70°$ and $\beta = 39.80°$, the change in δ, $\Delta\delta$, is minimal and less than 0.5°. Finally, δ is redefined as $\delta_{\text{new}} = 21.81°$. This value is the mean between δ_{max} and δ_{min}. Although this contradicts the relationship of Equation 3.5, δ_{new} ensures that compression and elongation of the crease $\overline{BC}$ are balanced.

Subsequent work will proceed using these optimized parameter values.

4. PROTOTYPE DESIGN AND MANUFACTURING

Building on the previously optimized geometry, this section describes the process of translating the design into a functional prototype and addresses the associated technical challenges.

One of the main challenges in transferring an origami-inspired structure to a technical application is accounting for material thickness. While paper's negligible thickness allows for ideal folding, technical structures require facets with significant thickness to enable force transmission. This consideration has already influenced the lower limit of γ. It also allows Tachi's approach to be applied, in which origami pattern creases serve as rotational axes and material is strategically removed from areas where intersections would otherwise occur [10].

This actuator uses hinges, as used by Shao et al. [11], in creases that transmit compressive forces for several reasons. They are durable and cannot be wedged between facets under compression. They also avoid brittleness over time, which could occur with flexible materials. However, since traditional hinges are not airtight, an air pouch must be inserted inside, as in Sadeghi et al.'s method [8]. The relative movement of the hinges must be considered, as it could damage the air pouch.

Since facets E and S are the largest facets of the actuator, they bear most of the force that needs to be transmitted to the end facets of the actuator. These compressive forces need to be transmitted via the creases, so these facets are connected via hinges. This results in numerous precisely aligned hinge axes across the entire actuator, necessitating tight production tolerances.

During small strokes, facet V becomes wedged between facets E and S. In order to accommodate the material thickness of facet V without any material intersection, the material from facets E and S must be moved out of their respective planes. This adjustment does not affect pneumatic performance. The force output remains unchanged, as long as the hinge axes remain correctly positioned. However, this modification results in less favorable internal load path within facets E and S, so these parts require reinforcement with support structures. Support structures on the inside of the actuator should be avoided to protect the air pouch.

These requirements, including hinged connections with precise positioning and small tolerances, out-of-plane material displacement, and reinforcement, result in highly complex components for facets E and S. Consequently, additive manufacturing is chosen for prototyping these parts. To be cost-efficient, FDM (fused deposition modeling) printing with PLA (polylactic acid) is used. However, the anisotropic mechanical properties resulting from print orientation must be considered, as demonstrated by Abdul Sani [12]. In general, to prevent hinge failure, the hinge axes should be perpendicular to the print layers. In case of this actuator, this orientation would expose parts of the components to perpendicular force transmission through the print layers, which could result in component failure. As a compromise, the components are printed at an angle (see Figure 4.1.). The wall thickness is set at $t = 4$ mm, and steel rods with a diameter of $d = 2$ mm are used as hinge axes. Given these choices in materials and manufacturing methods, maximum internal pressure is limited to $p_A = 1\ \mathrm{bar}_{rel}$. Support structures were iteratively improved under these conditions using an FEM (finite element method) simulation for facets E and S. The resulting parts for facet E and S are shown in Figure 4.1.. Figure 4.3. shows the parts assembled The dimensions corresponding to Figure 2.1. of the parts are $b_1 = 170$ mm and $b_2 = h = 50$ mm.

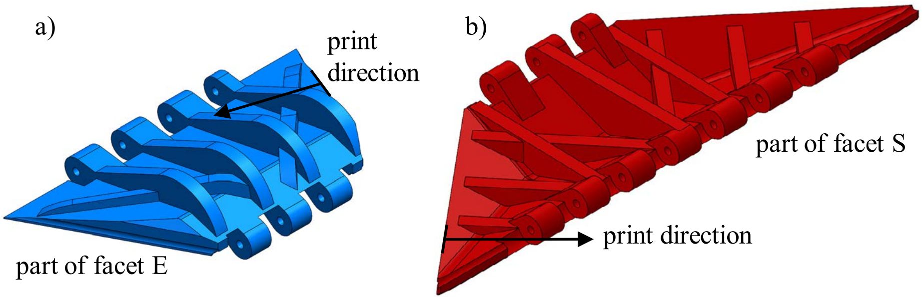

Figure 4.1. Parts of facet E and S, the shown print direction is perpendicular to print layers

A combination of steel and textile is used for both the hinges of facet V and the facet itself for several reasons. The fabric serves as a hinge, requiring significantly less space than a conventional mechanical hinge. These flexible fabric hinges are also well-suited for transmitting tensile forces, which are present along the outward-facing creases of facet V. A 1.5 mm sheet metal panel forms the main body of facet V, ensuring that it remains rigid and does not bulge under pressure. However, as it cannot accommodate for changes in δ, it is sandwiched between two layers of fabric. As the actuator operates, these fabric layers not only create the hinges but also compensate for variations in δ by stretching alongside the metal.

The sheet metal is held in place solely by stitching together the two surrounding fabric layers. In principle, combining the textile with an elastomer to form a composite material could make both facet V and its hinges airtight. Deleo et al. [13] and Zhakypov et al. [14] used similar approaches. However, since an air pouch is already used to achieve airtightness due to the non-sealing hinges on facets E and S, this additional step is unnecessary. Linen is selected as the textile because it allows controlled stretching, can efficiently transmit tensile forces, and remains thin enough for compact integration. The resulting structure of facet V is illustrated in Figure 4.2..

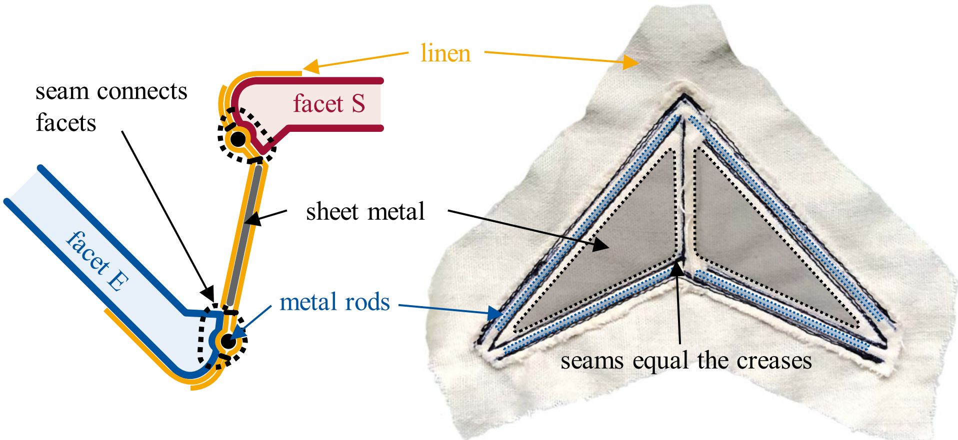

Figure 4.2. Design of facet V; Cross-section through facet E, V and S (left) and assembled facet V (right)

This design provides sufficient space for the air pouch while allowing facet V to fit between facets E and S throughout actuator movement. Metal rods, also enclosed within the two fabric layers of facet V, are stitched to facets E and S to connect facet V securely at both ends, as shown in Figure 4.2..

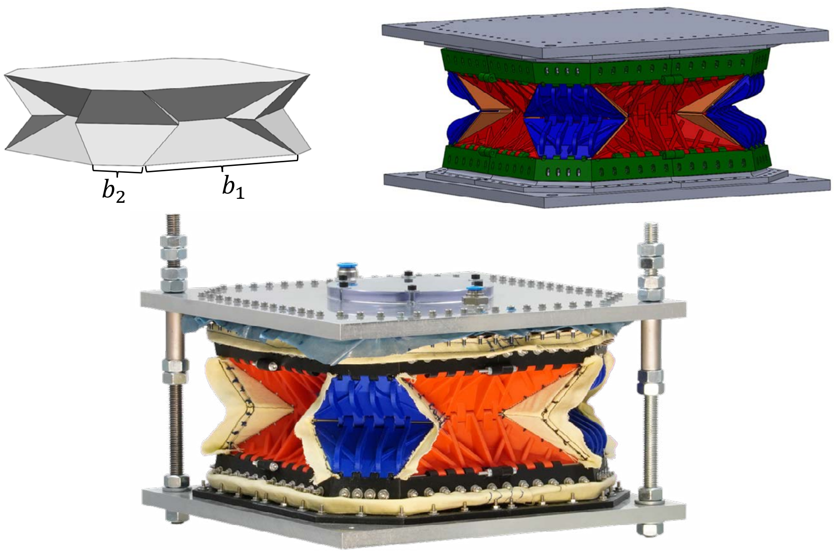

Figure 4.3. top: Origami-pattern and CAD-model of the prototype (screws are not shown); bottom: prototype of the actuator

Based on Sadeghi's approach, the actuator is sealed using a custom-made, tube-shaped air pouch made of 0.1 mm thick, low-density polyethylene film [8]. To protect the air pouch, all interior surfaces are kept flat with rounded corners and small gaps between parts. Additionally, a textile sleeve separates the moving origami elements from direct contact with the air pouch to prevent frictional wear or pinching, even when gaps open around moving joints. The air pouch's circumference exceeds what is needed. This ensures that the air pouch does not stretch but rather forms harmless folds of excess material.

Finally, the top and bottom of the actuator are closed off with 13 mm aluminum plates. These plates provide mounting points for mechanical and pneumatic connections. The air pouch is sandwiched between the printed origami parts and the aluminum plates. Silicone sealant ensures airtightness. Figure 4.3. illustrates the final prototype.

Like Tachi's approach, the rotational axes of the actuator correspond to the origami creases [10].

5. FORCE APPROXIMATION

Before conducting experimental investigations, the force-stroke characteristic of the developed actuator is first approximated mathematically. This preliminary analysis supports both the design of the testbed and the validation of subsequent measurement results.

To simplify the calculations, the origami structure is reduced to a two-dimensional bar model, as shown in Figure 5.1.. In this approximation, only facets E and S are considered. The contribution from facet V is neglected because its effect on the total output force is relatively small. The resulting pressure force of each facet F_{res} is concentrated at its centroid. Hereby z_s is the distance between the centroid and the hinge.

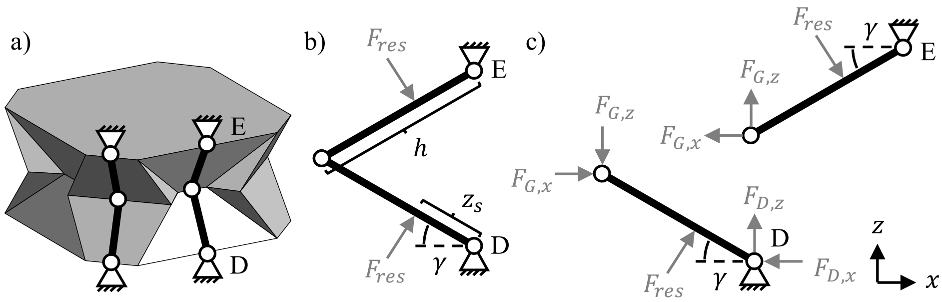

Figure 5.1. simplified mechanism for force approximation

The force $F_{G,z}$ can be determined for the lower and upper beams in Figure 5.1.c) if moment equilibrium is assumed at points D and E. Equating the two moment equilibria, it follows that $F_{G,z} = 0$. The force $F_{D,z}$ can be calculated using force equilibrium for the lower beam, as shown by Equation 5.1:

$$\Sigma F_z = 0 \Rightarrow F_{D,z} = -F_{res} \cdot \cos\gamma + F_{G,z} = F_{res} \cdot \left(\frac{z_s}{\cos\gamma \cdot h} - \cos\gamma\right) \quad (5.1)$$

The overall force generated by the actuator can then be expressed as shown in Equation 5.2:

$$F_{actuator} = 4 \cdot F_{D,z-facet\,S} + 4 \cdot F_{D,z-facet\,E} + F_{end\,face} \quad (5.2)$$

The force, $F_{end\ face}$, is the internal pressure multiplied by the area of the end face. The approximation of the actuator's output force will be used to validate the experimental results.

6. EXPERIMENTAL INVESTIGATION

To validate the proposed concept of an origami-inspired pneumatic actuator with a progressive force-stroke characteristic, this section describes the experimental procedures used to evaluate the previously designed prototype.

The primary focus of the experiments is to determine the force-stroke relationship of the actuator at constant internal pressures. To achieve this, a testbed is set up that can maintain a constant internal pressure, allow for variable stroke adjustments, and accurately measure the resulting force. Due to limitations of the available testing equipment, measurements can only be taken up to a maximum load of 5,000 N. This restricts the maximum internal pressure p_A during testing.

During each test series, the internal pressure of the actuator is set to an initial value of $0.05\ \text{bar}_{rel}$, which remains constant while the stroke is varied. The stroke is repeatedly decreased and increased three times before the internal pressure is raised by another increment of $0.05\ \text{bar}$. This process continues until the actuator's output force reaches 5,000 N. All measurements were recorded at a sampling rate of 1,000 Hz for high temporal resolution.

7. ACTUATOR CHARACTERIZATION

This section presents and analyzes the results obtained from experimental testing of the novel origami-inspired pneumatic actuator.

The previously described measurements were performed using the presented prototype. The maximum pressure is limited to $0.7\ \text{bar}_{rel}$ as the output force would otherwise exceed 5,000 N. For this reason, the maximum pressure for which the actuator is designed cannot be tested. To visualize the results, force is plotted against actuator stroke. The stroke x can be calculated from the angle γ. The angle $\gamma = [21°, 45.8°]$ corresponds to a stroke $x = [35.8\ \text{mm},\ 71.6\ \text{mm}]$ with the proposed dimensions of the prototype. To eliminate the influence of the end stops, x is set within the range of $x = [36.5\ \text{mm},\ 72.3\ \text{mm}]$. The lower end stop is defined by the actuator parts. The upper end stop can be set freely. Since the lower limit of x increased to eliminate the influence of the lower end stop, the upper limit is also raised to achieve the intended total stroke. In Figure 7.1. the force-stroke characteristic is exemplified for an internal pressure of $p_A = 0.3\ \text{bar}_{rel}$. To reduce measurement noise each data point is averaged over the previous 100 samples. This is acceptable because the stroke changes relatively slowly.

The resulting plot shows a hysteresis between increasing and decreasing stroke. The hinge friction could be the main cause of this effect. When retracting, frictional forces act in the same direction as the measured force. When extending, they oppose it. Consequently, measured force values are lower during extension than during retraction at any given stroke position.

Figure 7.1. also displays the approximated force curve for $p_A = 0.3\ \text{bar}_{rel}$ based on the previous calculations from section 5. Both the magnitude and trend of measured values closely match these theoretical predictions.

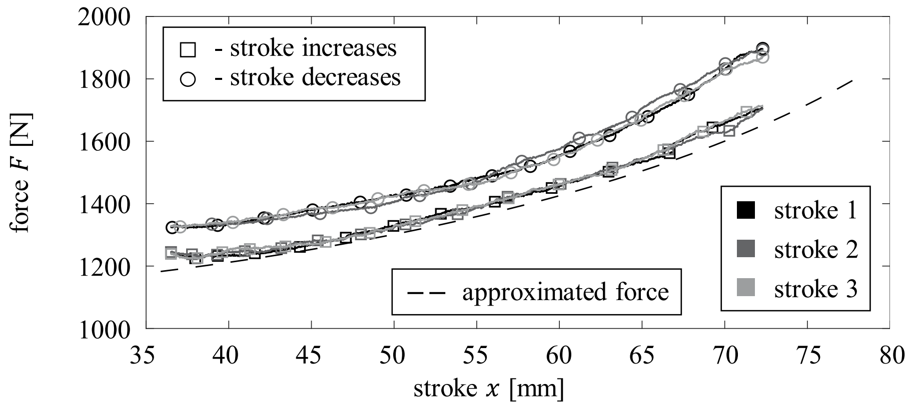

Figure 7.1. Actuator output force F plotted against actuator stroke x, with internal pressure $p_A = 0.3\ \text{bar}_{rel}$ and approximated force according to section 5

To further analyze performance and minimize the effect of pressure fluctuations during testing, each measured force value was divided by its corresponding pressure reading. The resulting "active area" metric A_{active} is proportional to the output force, yet independent of the pressure. These active area results for an internal pressure of $p_A = 0.3\ \text{bar}_{rel}$ are shown in Figure 7.2..

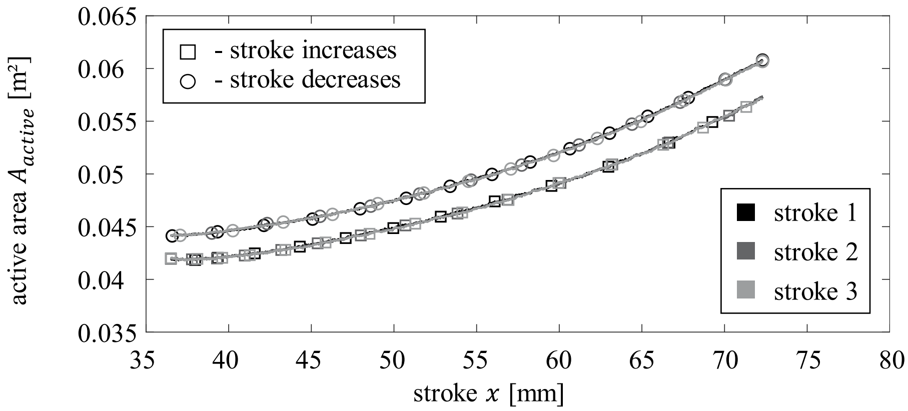

Figure 7.2. Active area A_{active} plotted against actuator stroke x, with internal pressure $p_A = 0.3\ \text{bar}_{rel}$

The three stroke cycles now align more closely with each other. This indicates that the previously observed fluctuations were largely due to minor variations in internal pressure rather than inconsistent actuator behavior.

The active area serves as a robust measure for comparing different pressure levels independently of the internal pressure. Figure 7.3. presents the active area of the actuator at different internal pressures. The internal pressure, p_A, ranges from 0.05 bar_{rel} to 0.7 bar_{rel} and describes the internal pressure of the actuator.

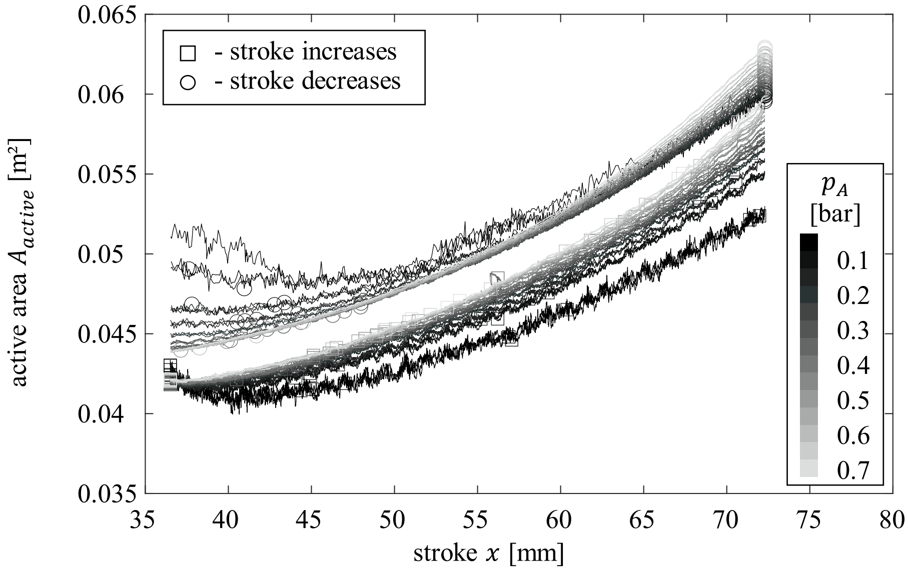

Figure 7.3. Active area A_{active} plotted against actuator stroke x, with different internal pressures p_A

At lower pressures, greater deviations are observed. These are likely because friction has a proportionally larger effect at low pressure. Friction could increase at low strokes, as the support structures of Facet E move closer together and rub against each other. At higher pressures the curves converge consistently. For strokes above approximately $x = 60$ mm, some divergence appears at higher pressures. This is likely due to stretching or deformation of parts under load, which results in minor changes in γ. These changes result in greater variations in output force at extended positions.

Overall, these results demonstrate that the actuator exhibits repeatable behavior and delivers a progressive force-stroke characteristic consistent with prior calculations.

8. Conclusion And Discussion

In this work, a novel origami-inspired pneumatic actuator concept featuring a progressive force-stroke characteristic was developed. An initial analysis of the geometric relationships served as a basis for the design and prototype implementation with minimized stretching of the facets.

The design uses 3D-printing. A textile-metal composite is used to achieve the necessary deformations in the actuator's facets. This approach allows the complex origami-geometry to be realized in a technical structure.

Experimental validation shows that the prototype works as intended. The measured force-stroke curves match the mathematically predicted progressive behavior. Results are consistent across multiple tests, showing that the actuator's performance is reproducible.

These findings confirm that it is possible to build an origami-based pneumatic actuator with a progressive force-stroke characteristic, by integrating flexible materials at key points.

Despite these achievements, high manufacturing effort remains a limitation due to complex components that require significant assembly effort. Future work can further develop this concept. Various origami-patterns could be explored to tailor pneumatic properties further based on usage requirements. Material selection and production methods can also be improved. Reducing manufacturing complexity and employing alternative materials for enhanced mechanical performance could facilitate the industrial use of such actuators. Potential applications include suspension systems or automation technology. In these fields, actuators with tailored force-stroke characteristics offer significant advantages. A simpler design could miniaturize the actuator, qualifying it for broader applications.

Overall, this study demonstrates both the feasibility and potential of origami-inspired pneumatic actuators for advanced engineering applications.

9. References

[1] R. J. Lang, 'The complete book of origami', Dover Publications Inc., New York, 1988. ISBN: 978-0-486-25837-9.

[2] S. Dixit, R. Hyde, A. Weisberg, J. Early, M. Rushford, J. Britten, 'Development of Large Aperture, Light-Weight Fresnel Lenses for Gossamer Space Telescopes', 43rd AIAA/ASME/ASCE/AHS/ASC Structures, Structural Dynamics, and Materials Conference, American Institute of Aeronautics and Astronautics, Reston, Virigina, 2002. https://doi.org/10.2514/MSDM02.

[3] K. Kuribayashi, K. Tsuchiya, Z. You, D. Tomus, M. Umemoto, T. Ito, M. Sasaki, 'Self-deployable origami stent grafts as a biomedical application of Ni-rich TiNi shape memory alloy foil', Materials Science and Engineering: A, pp. 131–137, 2006. https://doi.org/10.1016/j.msea.2005.12.016.

[4] S. Bhat, K. Heins, C. Bertram, O. Reinertz, K. Schmitz, T. Gries, 'Ein Ausblick auf das Zusammenspiel von Faltprozess und Drapierbarkeit der Textilbewehrung', Beton und Stahlbetonbau, pp. 925–935, Ernst & Sohn GmbH, 2024. https://doi.org/10.1002/best.202400062.

[5] L. M. Fonseca, G. V. Rodrigues, M. A. Savi, 'An overview of the mechanical description of origami-inspired systems and structures', International Journal of Mechanical Sciences, 2022. https://doi.org/10.1016/j.ijmecsci.2022.107316.

[6] O. Reinertz, 'Static Properties Based Classification of Pneumatic Actuators - Potential of Progressive Effective Area Over the Stroke', International Conference Fluid Power 2025: Conference Proceedings, pp. 111–130, University of Maribor Press, Maribor, 2025. https://doi.org/10.18690/um.fs.7.2025.

[7] S. Sadeghi, S. Li, 'Harnessing the Quasi-Zero Stiffness From Fluidic Origami for Low Frequency Vibration Isolation', Volume 2: Modeling, Simulation and Control of

Adaptive Systems; Integrated System Design and Implementation; Structural Health Monitoring, American Society of Mechanical Engineers, 2017. https://doi.org/10.1115/SMASIS2017-3754.

[8] S. Sadeghi, S. Li, ‘Fluidic origami cellular structure with asymmetric quasi-zero stiffness for low-frequency vibration isolation’, Smart Mater. Struct., 2019. https://doi.org/10.1088/1361-665X/ab143c.

[9] I. K. Sabitov, ‘On the problem of invariance of the volume of a flexible polyhedron’, Russ. Math. Surv., pp. 451-452, 1995. https://doi.org/10.1070/RM1995v050n02ABEH002095.

[10] T. Tachi, ‘Rigid-Foldable Thick Origami’, Origami 5, pp. 253–263, A K Peters/CRC Press, 2016. https://doi.org/10.1201/b10971.

[11] Z. Shao, W. Zhao, Z. Zuo, J. Li, I.-M. Chen, ‘An Origami-Inspired Negative Pressure Folding Actuator Coupling Hardness with Softness’, Actuators, p. 35, 2023. https://doi.org/10.3390/act12010035.

[12] A. S. Abdul Sani, M. N. Osman Zahid, M. R. Mohamad Yasin, S. Z. Ismail, M. Z. Mohd Zawawi, A. R. Abdul Manaf, S. N. Mohd Saffe, R. Abd Aziz, F. Mohd Turan, ‘Enabling Industry 4.0 through Advances in Manufacturing and Materials’, Springer Nature Singapore, Singapore, 2022. ISBN: 978-981-19-2889-5.

[13] A. A. Deleo, J. O’Neil, H. Yasuda, M. Salviato, J. Yang, ‘Origami-based deployable structures made of carbon fiber reinforced polymer composites’, Composites Science and Technology, 2020. https://doi.org/10.1016/j.compscitech.2020.108060.

[14] Z. Zhakypov, F. Heremans, A. Billard, J. Paik, ‘An Origami-Inspired Reconfigurable Suction Gripper for Picking Objects With Variable Shape and Size’, IEEE Robot. Autom. Lett., pp. 2894–2901, 2018. https://doi.org/10.1109/LRA.2018.2847403.

Biographies

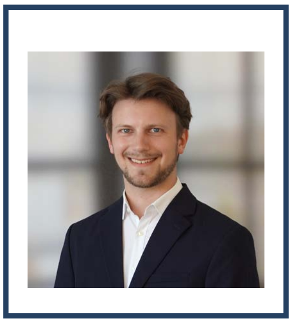

Philipp Hüpper received the bachelor's degree in mechanical engineering in 2022 and the master's degree in product development in 2025 from the RWTH Aachen University. He is currently working as a Research Associate at the Institute for Fluid Power Drives and Systems, Faculty of Mechanical Engineering, RWTH Aachen University. His research areas include Gas- and Micro-Systems with a special focus on high pressure hydrogen systems.

Prof. Olivier Reinertz received his diploma and his doctoral degree in mechanical engineering from RWTH Aachen University, Germany. He is currently Scientific Director at the Institute for Fluid Power Drives and Systems (ifas) at RWTH Aachen University. His research focuses on the model-based analysis of fluid power components and systems and the derivation and validation of innovative strategies for efficiency and performance optimization with an emphasis on compressed air and gas-powered systems.

Prof. Katharina Schmitz studied mechanical and chemical engineering at RWTH Aachen University and Carnegie Mellon University, Pittsburgh (USA) and graduated 2015 as Dr.-Ing. at RWTH Aachen University. Since 2018, she is full professor at RWTH Aachen University and director of the Institute for Fluid Power Drives and Systems (ifas). In addition, she is Vice Dean of the Faculty for Mechanical Engineering at RWTH Aachen, a position she holds since 2020. Prof. Schmitz's awards and honors include several best paper awards and 2023 IMechE Joseph Bramah Medal award.